RESEARCH ARTICLE

Estimation of Acoustic Channel Impulse Response at Low Frequencies Using Sparse Bayesian Learning for Nonuniform Noise Power

YOUNGMIN CHOO[1], **(Member, IEEE), AND HAESANG YANG**[2]**, (Member, IEEE)**

[1]Department of Defense System Engineering, Sejong University, Seoul 05006, South Korea
[2]Department of Naval Architecture and Ocean Engineering, Seoul National University, Seoul 08826, South Korea

Corresponding author: Haesang Yang (coupon3@snu.ac.kr)

ABSTRACT Sparse Bayesian learning (SBL) has been extended to estimate acoustic channel impulse responses (CIRs) at low frequencies, where matched filter (MF)-based CIR estimation suffers from low resolution due to a limited frequency band. In this study, the extended SBL was developed to account for nonuniform noise power in a signal model for the CIR via a formulation that considers inconsistent noise and multiple measurements, which cannot be handled in the conventional SBL. The extended SBL is applied to simulated and measured acoustic data and then compared with the MF and existing SBLs. With the advancement in the schemes, the time resolution and denoising are enhanced; especially, the results of the extended SBL on the simulated data show that it clearly distinguishes the two adjacent arrivals with moderate errors in the estimated time delays. Additionally, as a result of applying it to the measured array data, the extended SBL can achieve a high resolution in the CIR estimation, which retains assured arrivals with a single measurement, while some arrivals are weakened by the insufficient measurement for the extended SBL.

INDEX TERMS Acoustic channel impulse response, nonuniform noise distribution, sparse Bayesian learning, time-delay estimation.

I. INTRODUCTION

When a wave travels in a medium, the useful information of the medium between the source and receiver is embedded in channel impulse responses (CIRs) and transfer functions (TFs). Several applications, which include radar and sonar systems, exploit the CIR (or TF) for target-range estimation (time-delay estimation) and communication (channel parameter estimation) [1].

When a source waveform is known and its autocorrelation is compressed, a matched filter (MF), which correlates the source waveform with the received signal, is conventionally used for the CIR estimation. The MF improves the time resolution via the pulse compression and reduces noise that

The associate editor coordinating the review of this manuscript and approving it for publication was Yongming Li.

is uncorrelated with the source waveform, which is better for identifying the arrivals that compose of the CIR [2]. However, the time resolution is inversely proportional to the bandwidth of the source waveform, which restricts the application of the MF to high-frequency sources with broad bandwidths [3].

Compressive sensing (CS), which was expected to solve an underdetermined linear system by imposing a sparsity condition on the solution [4], [5], was used to improve the CIR estimation [6]. Ekanadham *et al.* [7] solved the linear system for CIRs using a modified CS, which is referred to as continuous basis pursuit (CBP), where time-shifted source waveforms are linearly combined to express the time-domain signal. The CBP that interpolates the time-shifted source waveforms by using the Taylor approximation or trigonometric spline outperforms the conventional CS which suffers from a basis mismatch caused by the arrivals with time delays

that do not belong to the time-shifted source waveforms. Fyhn *et al.* [8] estimated the amplitudes and the time delays of arrivals in the CIRs using a CS with polar interpolation, which outperformed the CBP.

In underwater acoustics, the CS has been predominantly applied to estimate the direction of arrivals (DOAs) from underwater targets [9], [10], [11], [12], [13], [15], [15] and was introduced in the underwater acoustic channel parameter estimation by several researchers [6], [16], [17], [18], whereas the MF-based CIR estimation is a conventional approach that was employed for active sonar systems [1], [2]. The sparse solutions in the CS literature help estimate the parameters with super-resolution [12], [17], [19]. However, manually determined hyperparameters in the schemes that are associated with measurement noise are sensitive to sparsity. They affect the performance of the schemes, which hinder their practical applications.

Sparse Bayesian learning (SBL) has been introduced to address the DOA or the channel parameter-estimation problem in underwater acoustics. The SBL was originally devised for classification and regression in machine learning [20]. In the SBL framework, the probability models for unknowns and measurement are derived using Bayesian inference with hyperparameters that are related to noise and source variances (or powers), which are automatically evaluated during the iterative process to update the probability models and the variances.

The SBL can be applied to determine a solution for a linear system, which is similar to the CS. The SBL has been primarily used for the DOA estimation in underwater acoustics due to its well-established linear system that relates DOAs with measurements along multiple sensors in an array. Furthermore, a sparse solution that was obtained via the SBL provides a high-resolution DOA with suppressed noise [21], [22], [23], [24], [25]. In the DOA estimation using the SBL, the standard SBL has been extended for more accurate and reliable evaluation of the DOAs using multiple measurements, the interpolation between the discretized bases, and complex noise models with different variances along the measurements [21], [22], [23], [26], [27]. In the SBL-based DOA estimation using multiple measurements, the common supports of the unknowns along multiple measurements (i.e., the estimated DOAs) have been found due to the arrivals having consistent directions over multiple measurements [23], [27].

An inherent limitation of the SBL-based scheme arises from the discretized bases, which leads to a basis mismatch. A signal representation via interpolation using adjacent bases around the true arrival in the off-grid direction was adopted to mitigate the basis-mismatch problem, and a mismatch from the predefined bases was evaluated during the iterative process in the SBL [21], [22]. Meanwhile, most studies that used the SBL operated on the basic assumption of uniform noise variance over the measurement. This assumption was relaxed by Gerstoft *et al.* [26] with an approximated updating rule for heteroscedastic noise, which enables the treatment of nonuniform noise with the SBL [27].

The CS has been previously used to estimate acoustic CIRs by utilizing the sparse arrivals in acoustic channels [6], [12], [16], [17], [19]. Meanwhile, the CS-based DOA estimations were recently advanced by the SBL, which can find the DOAs into sensor array without additional post-processing [21], [22], [23], [24], [25], [26], [27]. To the best of our knowledge, the SBL has not been used in estimating the CIRs. Thus, in this study, to extract the CIRs from a measurement (a signal emitted by a transducer, transmitted through the ocean waveguide, and received by a hydrophone), the SBL is adopted due to its properties that are exhibited in the DOA estimation as well as free manual hyperparameters and the properties of SBL are demonstrated in the CIR estimation.

A linear system for the CIR estimation is established by expressing the frequency domain, which is the TF and the candidate arrivals have distinct time delays. Note that noise in the linear system is scaled by the source spectrum, which results in nonuniform noise powers over the measurements that are relative to the frequency response of the received signal. The conventional SBL should be modified to accommodate the nonuniform noise, which was attempted by several researchers [26], [27], [28]. In the present study, a rigorous mathematical expression that accounts for the nonuniform noise is derived, and the associated updating rule is obtained, which is different from the previous studies by using the heuristic approach [26], [27] or considering only the real values and a single measurement [28]. Particularly, in [26] and [27], the previously established stochastic likelihood function was exploited, which provided an asymptotically efficient estimate of noise. To the best of our knowledge, no studies have been conducted on the SBL where the basic expressions for noise are rigorously extended for nonuniform noise to estimate the amplitudes and the time delays of arrivals in the CIRs. In Section II, the linear system for the CIRs is derived in the frequency domain using the definition of the TF. The conventional SBL is extended to account for the nonuniform noise powers in the linear system, which is discussed in Section III. The novel SBL is examined in terms of the time resolution enhancement and the noise reduction with simulated and measured acoustic data, which are shown in Sections IV and V, and the results are compared with the results from the MF and the existing SBLs. To investigate the performances of the conventional and the extended SBLs for uniform and nonuniform noise cases, we performed numerical experiments and discuss the validation regions of the SBLs. Section VI summarizes the present study.

II. UNDERWATER ACOUSTIC CHANNEL IMPULSE RESPONSE
A. ACOUSTIC CHANNEL IMPULSE RESPONSE USING AN MF

When underwater sound that is emitted from a source is transmitted through the ocean, the signal that arrives at the receiver contains multiple signals that pass through different paths that arise from the waveguide from the interfaces

(sea bottom and surface) and the scatterers (submerged objects and fish schools). An impulse response of the acoustic channel (acoustic CIR) is approximated by assuming an insignificant dispersion of acoustic waves during sound propagation (particularly, the Doppler effect is ignored because our attention is limited to the low frequency region), as follows [2], [6], [12], [16], [18], [19], [30]:

$$h(t) = \sum_{k=1}^{K} a_k \delta(t - \tau_k), \tag{1}$$

where a_k and τ_k are the amplitude and time delay of arrival, respectively, and K is the number of (dominant) arrivals. The received signal, $y(t)$, is represented by the convolution between the source waveform $s(t)$ and the acoustic CIR $h(t)$ with ubiquitous noise $n(t)$ as follows:

$$y(t) = \sum_{k=1}^{K} a_k s(t - \tau_k) + n(t). \tag{2}$$

A known source waveform is exploited to estimate the CIR when operating an active sonar system, which uses a transducer and a receiver that have almost flat frequency responses in the source bandwidth. By using the Fourier transform (FT), (2) is denoted in the frequency domain as follows:

$$Y(\omega) = S(\omega) H(\omega) + N(\omega), \tag{3}$$

where $S(\omega)$, $H(\omega)$, and $Y(\omega)$ are the FTs of the source waveform, CIR, and received signal, respectively. For a received signal without noise, the CIRs can be obtained via the inverse FT of $Y(\omega)/S(\omega)$. However, the CIR cannot be directly evaluated due to the ubiquitous noise, $N(\omega)$. Alternatively, an MF using cross-correlation between the source and the received signals is applied to estimate the CIR. The MF exhibits both advantages in regards to distinguishing the arrivals and enhancing the SNR by exploiting the frequency band of the source signal (pulse compression), whereas its performance is degraded at low frequencies due to the utilization of a limited frequency band.

B. ACOUSTIC CHANNEL ESTIMATION USING SBL
To overcome the limitation of the MF, an SBL applicable to solve a linear system is used for a high-resolution CIR estimation at low frequencies that uses its sparse solution. The linear system in this study is derived with the approximation of $H(\omega)$ in (3) as follows [2], [6], [12], [16], [18], [19], [30]:

$$\hat{Y}(\omega) = H(\omega) + \widehat{N}(\omega) \approx \sum_{n=1}^{N} x_n e^{-j\omega n \Delta \tau} + \widehat{N}(\omega), \tag{4}$$

where $\hat{Y}(\omega)$ and $\widehat{N}(\omega)$ are $Y(\omega)/S(\omega)$ and $N(\omega)/S(\omega)$, respectively. For the approximation, the time delay in the continuous domain is discretized with the grid of $\Delta \tau$, which is equal to $1/f_s$, where f_s is the sampling frequency and $N\Delta\tau$ the largest observation time of the received signal. When $n\Delta\tau$ in (4) matches τ_k in (1) with a sufficiently fine grid, the corresponding amplitude x_n is equivalent to a_k; otherwise, x_n becomes zero. The number of non-zero elements is the number of arrivals K. By arranging (4) according to the

source frequency band, the linear system is established as follows:

$$\begin{pmatrix} \hat{Y}_1 \\ \vdots \\ \hat{Y}_M \end{pmatrix} = \begin{pmatrix} e^{-j\omega_1 \Delta\tau} & \cdots & e^{-j\omega_1 N \Delta\tau} \\ \vdots & \ddots & \vdots \\ e^{-j\omega_M \Delta\tau} & \cdots & e^{-j\omega_M N \Delta\tau} \end{pmatrix} \begin{pmatrix} x_1 \\ \vdots \\ x_N \end{pmatrix}$$
$$+ \begin{pmatrix} \widehat{N}_1 \\ \vdots \\ \widehat{N}_M \end{pmatrix}. \tag{5}$$

Equation (5) is rearranged by adopting the following vector and matrix notation: $y = \mathbf{A}x + n$, where y, x, n, and $\mathbf{A}$ are the measurement, unknown, noise, and transformation matrix, respectively. It is worth noting that the signal model cannot be in the form of a linear system without dividing $S(\omega)$ in (3), because the corresponding unknown that has $S(\omega) x_n$ as an element varies according to the equality conditions. The measurement element $\hat{Y}_m$ and the noise element $\widehat{N}_m$ are $\hat{Y}(\omega)$ and $\widehat{N}(\omega)$ at the angular frequency ω_m, respectively. ω_1 and ω_M correspond to the lowest and highest frequencies, respectively, which are used for the SBL-based CIR estimation and belong to the source frequency band. The number of equations, M, is smaller than the number of unknowns, N. The SBL is used to determine a solution of the underdetermined linear system (i.e., the amplitudes and the time delays of arrivals that constitute of the CIR).

In contrast, a linear system can be constructed in the time domain, where the transformation matrix comprises of the time-shifted source waveforms as its columns and M is equal to N. In this study, the solution of the frequency domain linear system is preferred because less equality conditions cause a more refined CIR with a sparser solution by recovering less meaningful arrivals than the given equality conditions.

Note that the noise powers in (5) (i.e., variances of $\widehat{N}_m$) are inconsistent due to the fluctuating ocean noise spectrum being scaled by the source spectrum [29], which violates the assumption of constant noise power over the measurements in the conventional SBL [20]. Therefore, the conventional SBL should be modified to treat the nonuniform noise powers, which is described in the following section. Hereafter, the conventional and expanded SBL are referred to as uniform noise SBL (UN-SBL) and nonuniform noise SBL (NN-SBL), respectively.

III. SBL FOR NONUNIFORM NOISE POWER
An SBL was first introduced by Tipping [20] for classification and regression in machine learning. It was later adopted for high-resolution beamforming in underwater acoustics, where noise powers over measurements (frequency domain signals at sensors in array) are assumed to be constant, as in the original paper, except for a few studies [26], [27], where the formulations in the SBL were modified approximately to treat the nonconstant noise. However, in this study, the SBL is rigorously expanded by deriving mathematical expressions for the probabilities in the SBL for inconsistent noise powers

regarding complex value and multiple measurements. Afterwards, the results for the SBL using different approaches for the nonconstant noise are compared with each other.

In the SBL framework, the unknown (x) and noise (n) are treated as random vectors, which consist of independent random variables, and they are assumed to follow a zero-mean Gaussian distribution that has different variances (or different powers), which are hidden variables inferred using measurement (y). A linear system in the SBL is solved by finding x, which maximizes the probability as follows [20]:

$$
\begin{aligned}
x_{est} &= \underset{x}{\arg\max}\ p\left(x, \gamma_s, \gamma_n | y\right) \\
&= \underset{x}{\arg\max}\ p\left(x | y, \gamma_s, \gamma_n\right) p\left(\gamma_s, \gamma_n | y\right). \quad (6)
\end{aligned}
$$

In this study, γ_s is a vector that comprises of the signal powers along the time delays, and γ_n is a vector that comprises of the noise powers along the frequencies that belong to the source frequency band. Unlike the previous studies [20], [21], [22], [23], a constant noise power in the UN-SBL is replaced with vector γ_n in the NN-SBL to account for the different noise variances over the source frequency band. As displayed in the second line in (6), the estimation is conducted in two phases. First, using a given measurement y, the variances are obtained by maximizing $p\left(\gamma_s, \gamma_n | y\right)$, which is equivalent to maximizing $p\left(y | \gamma_s, \gamma_n\right)$ when γ_s and γ_n are uniformly distributed, which is the situation in this study, and there are no preferences for specific components in γ_s and γ_n [20]. The solution x_{est} is then obtained with the maximum a posteriori estimate of $p\left(x | y, \gamma_s, \gamma_n\right)$ using the measurement with the variances from the previous phase.

A. PROBABILITY MODELS FOR NN-SBL
The NN-SBL starts by deriving an analytic expression for the posterior probability $p\left(x | y, \gamma_s, \gamma_n\right)$, which is denoted below using Bayes' theorem:

$$
p\left(x | y, \gamma_s, \gamma_n\right) = \frac{p\left(y | x, \gamma_n\right) p\left(x | \gamma_s\right)}{p\left(y | \gamma_s, \gamma_n\right)}, \quad (7)
$$

where $p\left(y | x, \gamma_n\right)$ is the likelihood function, and $p\left(x | \gamma_s\right)$ is the prior function. Furthermore, $p\left(y | \gamma_s, \gamma_n\right)$ is the evidence (marginal likelihood) that is used to evaluate the hidden variables of the variances.

The noise is an independent random variable that follows a zero-mean circularly symmetric complex Gaussian distribution, so the likelihood function is expressed as follows using the relation between the measurement and the noise, which is based on (5):

$$
\begin{aligned}
p\left(y | x, \gamma_n\right) &= \frac{1}{\pi^M \prod_{m=1}^{M} (\gamma_n)_m} \\
&\times \exp\left\{ -\sum_{m=1}^{M} \frac{|(y - Ax)_m|^2}{(\gamma_n)_m} \right\} \\
&= \frac{1}{\pi^M |\Gamma_n|} \exp\left\{ -(y - Ax)^H \Gamma_n^{-1} (y - Ax) \right\}, \\
& \hspace{8.5cm} (8)
\end{aligned}
$$

where $(v)_m$ and $(v)^H$ denote the mth element and the conjugate transpose (or Hermitian transpose) of vector v, respectively. Γ_n is a diagonal matrix that results from the independent noise making off-diagonal components zeros, and its diagonal components are γ_n (i.e., $\Gamma_n = \text{diag}(\gamma_n)$).

The prior corresponds to the distribution of the unknown comprising independent random variables as follows:

$$
\begin{aligned}
p\left(x | \gamma_s\right) &= \frac{1}{\pi^N \prod_{n=1}^{N} (\gamma_s)_n} \exp\left\{ -\sum_{m=1}^{M} \frac{(x)_n^2}{(\gamma_s)_n} \right\} \\
&= \frac{1}{\pi^N |\Gamma_s|} \exp\left(-x^H \Gamma_s^{-1} x \right), \quad (9)
\end{aligned}
$$

where Γ_s is a diagonal matrix whose diagonal components equal γ_s (i.e., $\Gamma_s = \text{diag}(\gamma_s)$). The components of x are activated when the corresponding components of γ_s have non-zero values. During the application of the SBL for solving the linear system, γ_s appears sparsely, which is advantageous to enhance the resolution and suppressing noise [21], [22], [23], [26], [27].

The evidence can be derived using γ_s and γ_n with a linear system. The Gaussian-distributed unknown and noise in the linear system render the evidence normally distributed as follows:

$$
p\left(y | \gamma_s, \gamma_n\right) = \frac{1}{\pi^M |\Sigma_y|} \exp\left(-y^H \Sigma_y^{-1} y \right). \quad (10)
$$

The mean of y is equal to a zero vector because each mean of the unknown and noise is the zero vector, $\langle y \rangle = A\langle x \rangle + \langle n \rangle = 0$. Σ_y is calculated with the definition of the covariance matrix as follows:

$$
\Sigma_y = \langle (Ax + n)(Ax + n)^H \rangle = A\Gamma_s A^H + \Gamma_n. \quad (11)
$$

Note that the nonuniform noise power leads to different forms of the likelihood function and the evidence from them in the UN-SBL, which subsequently result in a distinct posterior probability.

By substituting (8)–(10) in (7), the posterior probability that considers the inconsistent noise variances is derived using the Woodbury matrix identity as follows:

$$
\begin{aligned}
p\left(x | y, \gamma_s, \gamma_n\right) &= \frac{1}{\pi^N |\Sigma_x|} \\
&\times \exp\left\{ -\left(x - \mu_x\right)^H \Sigma_x^{-1} \left(x - \mu_x\right) \right\}, \\
& \hspace{8cm} (12)
\end{aligned}
$$

where $\Sigma_x = \left(\Gamma_s^{-1} + A^H \Gamma_n^{-1} A \right)^{-1}$ and $\mu_x = \Sigma_x A^H \Gamma_n^{-1} y$. As expected, the posterior probability follows a Gaussian distribution, and its mean and covariance matrix are calculated using the estimated γ_s and γ_n with measurement y. x_{est} is equivalent to μ_x, where the posterior probability is the maximum.

B. ESTIMATE OF THE VARIANCES γ_s AND γ_n
As previously described, γ_s and γ_n must be estimated to obtain the solution via the SBL. The variances that best

describe the given measurement are used for the solution, and they are calculated as follows:

$$(\check{\gamma}_s, \check{\gamma}_n) = \underset{\gamma_s, \gamma_n}{\arg\max}\ p\left(\gamma_s, \gamma_n \mid y\right). \quad (13)$$

$p\left(\gamma_s, \gamma_n \mid y\right)$ equals $p\left(y \mid \gamma_s, \gamma_n\right) p\left(\gamma_s\right) p\left(\gamma_n\right)$. When there are no preferences over the signal and noise, which is the situation in this study (i.e., both $p\left(\gamma_s\right)$ and $p\left(\gamma_n\right)$ follow a uniform distribution) [20], (13) becomes the same problem of finding γ_s and γ_n to maximize $p\left(y \mid \gamma_s, \gamma_n\right)$ as follows:

$$(\check{\gamma}_s, \check{\gamma}_n) = \underset{\gamma_s, \gamma_n}{\arg\max}\ p\left(y \mid \gamma_s, \gamma_n\right). \quad (14)$$

Herein, the expectation-maximization (EM) algorithm is applied to estimate γ_s and γ_n, where x is treated as a latent variable. The formulation for the EM-based estimation is as follows [20], [21], [22]:

$$\begin{aligned} Q\left(\gamma_s, \gamma_n\right) &= E_{x|y,\gamma_s,\gamma_n}\left\{\ln p\left(y, x | \gamma_s, \gamma_n\right)\right\} \\ &= E_{x|y,\gamma_s,\gamma_n}\left\{\ln p\left(x|\gamma_s\right) p\left(y|x,\gamma_n\right)\right\}. \end{aligned} \quad (15)$$

Equation (15) is equivalent to (14). The second line enables the variances to be estimated separately, so the conditional probabilities for x and y are used to evaluate γ_s and γ_n, respectively.

The expectation of $\ln p\left(x|\gamma_s\right)$ in the perspective of the posterior probability is stated as follows, which omits the terms that are irrelevant to γ_s:

$$\begin{aligned} Q_s\left(\gamma_s\right) &= -\ln|\Gamma_s| - \langle x^H \Gamma_s^{-1} x\rangle \\ &= -\ln|\Gamma_s| - \text{tr}\left\{\Gamma_s^{-1}\left(\Sigma_x + \mu_x \mu_x^H\right)\right\}, \end{aligned} \quad (16)$$

where $\text{tr}\left(M\right)$ is the trace of matrix M. γ_s is achieved by determining the vector that corresponds to the maximum of $Q_s\left(\gamma_s\right)$ as follows:

$$\left(\gamma_s\right)_n = \left(\Sigma_x\right)_{nn} + \left|\left(\mu_x\right)_n\right|^2. \quad (17)$$

M_{nn} is the nth diagonal component of the matrix M. Using (17), γ_s (or Γ_s) is computed element-wise.

The expectation of $\ln p\left(y|x, \gamma_n\right)$ from the perspective of the posterior probability is denoted as follows, which the terms relevant to γ_n are retained:

$$\begin{aligned} Q_n\left(\gamma_n\right) &= -\ln|\Gamma_n| - \langle(y - Ax)^H \Gamma_n^{-1}(y - Ax)\rangle \\ &= -\ln|\Gamma_n| - \left(y - A\mu_x\right)^H \Gamma_n^{-1}\left(y - A\mu_x\right) \\ &\quad - tr\left(\Sigma_x A^H \Gamma_n^{-1} A\right). \end{aligned} \quad (18)$$

The extremum of the function $Q_n\left(\gamma_n\right)$ is obtained as follows:

$$\left(\gamma_n\right)_m = \left|\left(y - A\mu_x\right)_m\right|^2 + A_{m:}\Sigma_x A_{m:}^H, \quad (19)$$

where $M_{m:}$ is mth row of matrix M. The noise variance $\left(\gamma_n\right)_m$ is the noise power in the mth measurement, and it comprises of two terms. The first is about the difference between the mth measurement and the associated estimation, and the other is related to the remnant weighted by the mth row of the transformation matrix. When the noise powers have the same

value as in the UN-SBL, the constant noise power $\bar{\gamma}_n$ is expressed as follows:

$$\bar{\gamma}_n = \frac{1}{M}\left\{\|y - A\mu_x\|_2^2 + \text{tr}\left(A\Sigma_x A^H\right)\right\}. \quad (20)$$

$\|v\|_2$ is the Euclidean norm of the vector v. This is the average of the noise powers over the measurement (i.e., $\bar{\gamma}_n = \sum_{m=1}^M \left(\gamma_n\right)_m /M$) and it equals the previous result ((22) in Ref. [21] for a single measurement). The noise power was previously estimated with a representative value as the average, whereas, the power was expressed individually according to the measurement component in this study. When the variation of the noise powers is noticeable, (19) should accommodate the probabilities of y, which was considered in this study. This is achieved at the cost of the increased number of variables (the noise variances), and it is proportional to the equality conditions in (5).

To estimate γ_s and γ_n, the posterior probability $p\left(x \mid y, \gamma_s, \gamma_n\right)$ (or μ_x and Σ_x) is required, and it is expressed using γ_s and γ_n with the measurement, which they are entangled to each other. Thus, the first step in the EM algorithm is to generate $p\left(x \mid y, \gamma_s, \gamma_n\right)$ with initial small values γ_s and γ_n (initial guesses for γ_s and γ_n), which allows Σ_x to be non-singular. In the next step, using μ_x and Σ_x in the posterior probability, $\check{\gamma}_s$ and $\check{\gamma}_n$ are computed using (17) and (19), respectively, which are used to update the posterior probability. The expectation and maximization steps are iterated until convergence, and they correspond to the first and second terms in the second line of (6). The final $\check{\gamma}_s$ and $\check{\gamma}_n$ are used to evaluate x_{est}, which is equivalent to the final μ_x.

C. EXTENSION OF NN-SBL FOR MULTIPLE MEASUREMENTS

Unlike the previous studies [20], [21], [22], [23], the noise power is estimated using the corresponding element in the measurement vector, which reduces the performance of the NN-SBL at low SNRs. To alleviate this problem, multiple measurements can be exploited when the underwater sounds are repeatedly emitted from a transducer for a relatively short duration or in a stationary ocean environment.

The NN-SBL that uses a single measurement has been expanded to exploit the common time delays of arrivals over the multiple measurements [22], [23]. The first step for the expansion is to modify the posterior probability to accommodate the multiple measurements as follows:

$$p\left(X \mid Y, \gamma_s, \gamma_n\right) = \frac{p\left(Y \mid X, \gamma_n\right) p\left(X \mid \gamma_s\right)}{p\left(Y \mid \gamma_s, \gamma_n\right)}, \quad (21)$$

where the measurement matrix Y comprises of the measurement vectors as its columns and an unknown matrix X comprises of the corresponding unknown vectors $Y = [y_1, \ldots, y_L]$ and $X = [x_1, \ldots, x_L]$. L is the number of measurements that are used for the estimation. The random vectors of x_l and y_l are assumed to be independent of each

other, and the likelihood function, which is the prior probability, and evidence for multiple measurements can then be stated as follows:

$$
\begin{aligned}
p\left(\mathbf{Y} \mid \mathbf{X}, \boldsymbol{\gamma}_n\right) = \prod_{l=1}^{L} & \frac{1}{\pi^M \left|\boldsymbol{\Gamma}_n\right|} \\
& \times \exp\left\{-\left(\mathbf{y}_l - \mathbf{A}\mathbf{x}_l\right)^H \boldsymbol{\Gamma}_n^{-1}\left(\mathbf{y}_l - \mathbf{A}\mathbf{x}_l\right)\right\}.
\end{aligned}
\tag{22}
$$

$$
p\left(\mathbf{X} \mid \boldsymbol{\gamma}_s\right) = \prod_{l=1}^{L} \frac{1}{\pi^N \left|\boldsymbol{\Gamma}_s\right|} \exp\left(-\mathbf{x}_l^H \boldsymbol{\Gamma}_s^{-1} \mathbf{x}_l\right). \tag{23}
$$

$$
p\left(\mathbf{Y} \mid \boldsymbol{\gamma}_s, \boldsymbol{\gamma}_n\right) = \prod_{l=1}^{L} \frac{1}{\pi^M \left|\boldsymbol{\Sigma}_y\right|} \exp\left(-\mathbf{y}_l^H \boldsymbol{\Sigma}_y^{-1} \mathbf{y}_l\right). \tag{24}
$$

The measurement $\mathbf{y}_l$ and the corresponding unknown $\mathbf{x}_l$ vary over the duration of the measurement due to noise and subtle variations in the ocean environment. However, $\boldsymbol{\Gamma}_n$, $\boldsymbol{\Gamma}_s$, and $\boldsymbol{\Sigma}_y$ (or $\boldsymbol{\gamma}_s$ and $\boldsymbol{\gamma}_n$) remain constant (hereafter, subscript l indicates the dependence of the measurement). By substituting (22)–(24) in (21), the posterior probability for the multiple measurements is derived as follows:

$$
\begin{aligned}
p\left(\mathbf{X} \mid \mathbf{Y}, \boldsymbol{\gamma}_s, \boldsymbol{\gamma}_n\right) = \prod_{l=1}^{L} & \frac{1}{\pi^N \left|\boldsymbol{\Sigma}_x\right|} \\
& \times \exp\left\{-\left(\mathbf{x}_l - \boldsymbol{\mu}_{\mathbf{x}_l}\right)^H \boldsymbol{\Sigma}_x^{-1}\left(\mathbf{x}_l - \boldsymbol{\mu}_{\mathbf{x}_l}\right)\right\}.
\end{aligned}
\tag{25}
$$

$\boldsymbol{\mu}_{\mathbf{x}_l}$ is the lth column of $\boldsymbol{\mu}_{\mathbf{X}} = \boldsymbol{\Sigma}_x \mathbf{A}^H \boldsymbol{\Gamma}_n^{-1} \mathbf{Y}$: $\boldsymbol{\mu}_{\mathbf{x}_l} = \boldsymbol{\Sigma}_x \mathbf{A}^H \boldsymbol{\Gamma}_n^{-1} \mathbf{y}_l$. As in the single-measurement SBL, the posterior probability is used for deriving $\check{\boldsymbol{\gamma}}_s$ and $\check{\boldsymbol{\gamma}}_n$.

Updating rules for $\check{\boldsymbol{\gamma}}_s$ and $\check{\boldsymbol{\gamma}}_n$ in the multiple measurement SBL are based on the expectations of $\ln p\left(\mathbf{X} \mid \boldsymbol{\gamma}_s\right)$ and $\ln p\left(\mathbf{Y} \mid \mathbf{X}, \boldsymbol{\gamma}_n\right)$ from the perspective of the posterior probability, respectively, and their maxima are at $\boldsymbol{\gamma}_s$ and $\boldsymbol{\gamma}_n$, as follows:

$$
\left(\boldsymbol{\gamma}_s\right)_n = \left(\boldsymbol{\Sigma}_x\right)_{nn} + \frac{1}{L}\left\|\left(\boldsymbol{\mu}_{\mathbf{X}}\right)_{n:}\right\|_2^2. \tag{26}
$$

$$
\left(\boldsymbol{\gamma}_n\right)_m = \frac{1}{L}\left\|\left(\mathbf{Y} - \mathbf{A}\boldsymbol{\mu}_{\mathbf{X}}\right)_{m:}\right\|_2^2 + \mathbf{A}_{m:}\boldsymbol{\Sigma}_x \mathbf{A}_{m:}^H. \tag{27}
$$

As shown in (26) and (27), the means of the signal and the noise powers over multiple measurements are used for the update, which benefits the estimation at low SNRs. In contrast, the average of the noise variances over frequency components and multiple measurements can be used to derive the updating rule for the uniform noise power case as follows:

$$
\bar{\gamma}_n = \frac{1}{M}\left\{\frac{1}{L}\left\|\mathbf{Y} - \mathbf{A}\boldsymbol{\mu}_{\mathbf{X}}\right\|_F^2 + \operatorname{tr}\left(\mathbf{A}\boldsymbol{\Sigma}_x \mathbf{A}^H\right)\right\}, \tag{28}
$$

where $\|\mathbf{M}\|_F$ is the Frobenius norm of matrix $\mathbf{M}$.

When multiple measurements are exploited, $\boldsymbol{\mu}_{\mathbf{X}}$ obtained using $\check{\boldsymbol{\gamma}}_s$ and $\check{\boldsymbol{\gamma}}_n$ from the EM algorithm, which comprises columns that have non-zero elements at the same locations. In the SBL using multiple measurements, $\mathbf{x}_{est}$ is computed with the average of $\boldsymbol{\mu}_{\mathbf{X}}$ along the measurements (column axis), and the shared common supports improve the robustness of the NN-SBL.

TABLE 1. NN-SBL algorithm.

Initialize: $\boldsymbol{\gamma}_s = 0.001$, $\boldsymbol{\gamma}_n = 0.001$, $\epsilon_{\min} = 10^{-5}$, $j_{\max} = 200$

1	while $(\epsilon > \epsilon_{\min})$ and $(j < j_{\max})$
2	$j = j + 1, \boldsymbol{\gamma}_s^{\text{old}} = \boldsymbol{\gamma}_s^{\text{new}}, \boldsymbol{\gamma}_n^{\text{old}} = \boldsymbol{\gamma}_n^{\text{new}}, \boldsymbol{\Gamma}_s = \operatorname{diag}(\boldsymbol{\gamma}_s^{\text{new}}),$ $\boldsymbol{\Gamma}_n = \operatorname{diag}(\boldsymbol{\gamma}_n^{\text{new}})$
3	$\boldsymbol{\Sigma}_x = (\boldsymbol{\Gamma}_s^{-1} + \mathbf{A}^H \boldsymbol{\Gamma}_n^{-1}\mathbf{A})^{-1}$
4	$\boldsymbol{\mu}_x = \boldsymbol{\Sigma}_x \mathbf{A}^H \boldsymbol{\Gamma}_n^{-1}\mathbf{y}$
5	$(\boldsymbol{\gamma}_s^{\text{new}})_n = (\boldsymbol{\Sigma}_x)_{nn} + |(\boldsymbol{\mu}_x)_n|^2$ (17)
6	$(\boldsymbol{\gamma}_n^{\text{new}})_m = |(\mathbf{y} - \mathbf{A}\boldsymbol{\mu}_x)_m|^2 + \mathbf{A}_{m:}\boldsymbol{\Sigma}_x \mathbf{A}_{m:}^H$ (19)
7	$\epsilon = \left\|\boldsymbol{\gamma}_s^{\text{new}} - \boldsymbol{\gamma}_s^{\text{old}}\right\|_2 / \left\|\boldsymbol{\gamma}_s^{\text{old}}\right\|_2$
8	Output: $\boldsymbol{\mu}_x, \boldsymbol{\gamma}_s^{\text{new}}, \boldsymbol{\gamma}_n^{\text{new}}$

IV. PERFORMANCE OF THE CHANNEL IMPULSE RESPONSE ESTIMATOR USING NONUNIFORM NOISE SBL

A. IDEAL TF WITH UNIFORM AND NONUNIFORM NOISE POWER

The performance of the CIR estimator using the NN-SBL is examined using simulated data that considers two different situations with constant and nonconstant noise variances in the measurements. When generating synthetic data (measurement), an ideal TF using (5) neglecting acoustic wave distortion during propagation is applied, and the time delay of arrival is on the grid of the observation time discretized with a sampling frequency. This experimental setup allows for the direct performance demonstration of the SBL-based CIR estimator according to the SNR, which excludes the pulse distortion and the basis-mismatch effects on the estimator, which is shown in the later numerical experiments.

A single arrival is presumably in a received signal for the convenient evaluation of the errors from the SBLs. The longest observation time was 200 ms, and the signal with a frequency band between 250 Hz and 750 Hz, which correspond to the lowest and highest frequencies in (5), respectively, randomly arrives between 20 ms and 180 ms in the simulation. The ideal TF without noise is produced with the transformation matrix multiplied by $\mathbf{x}$, which comprises of a single non-zero element (value of one) that corresponds to the random arrival time. The transformation matrix is formed with the discretized time delays (along columns) and the angular frequencies (along rows) using a sampling frequency of 3,000 Hz (four times the maximum frequency). There are 601 unknowns (N) and 100 equality conditions (M).

The following noise is added to the noise-free ideal TF to examine the robustness of the SBL-based estimator.

$$
\widehat{N}_{m,l} = \widehat{N}_P\left(\omega_m\right)\left\{U\left(-0.5, +0.5\right) + iU\left(-0.5, +0.5\right)\right\}, \tag{29}
$$

where $U(a, b)$ is the uniform distribution between a and b. The subscripts m and l denote the lth measurement at ω_m. $\widehat{N}_P\left(\omega_m\right)$ determines the SNR of the measurement at ω_m. The noise variances are constant over multiple measurements due to the stationary ocean environment, so $\widehat{N}_P\left(\omega_m\right)$ is independent of the measurement time (or measurement number l). For a simulation with uniform noise power, $\widehat{N}_P\left(\omega_m\right)$ becomes
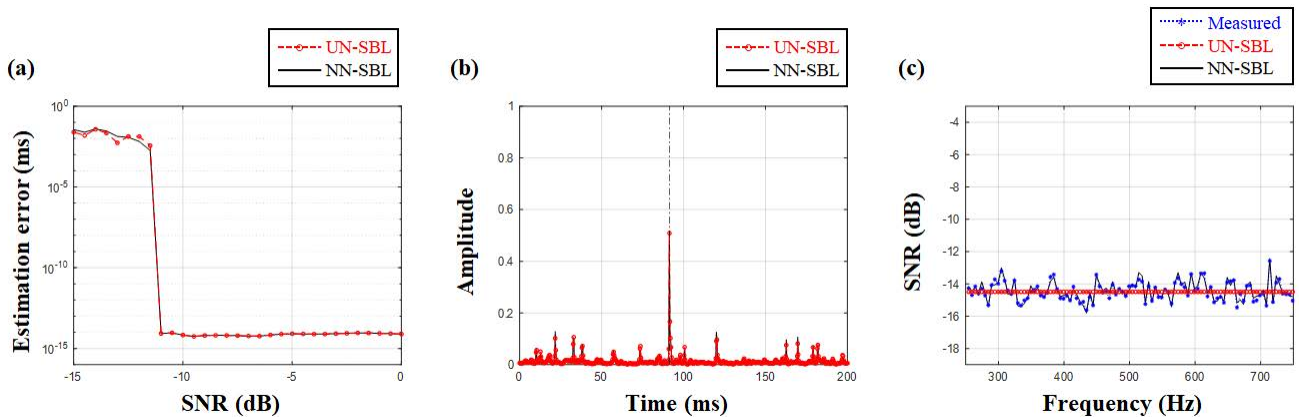
FIGURE 1. The conventional and the extended sparse Bayesian learning (UN-SBL and NN-SBL) using simulated data, which included noise with constant variance over measurements along the frequency. An ideal transfer function is used for the simulation. (a) The mean estimation error evaluated by the difference between the true and the estimated time delays. (b) Channel impulse responses from the SBLs at an SNR of approximately −14 dB. The vertical dash-dotted line indicates the true arrival. (c) The corresponding noise variances along the frequency, which are compared to the measured noise variances using (30).

constant over the angular frequencies as well as the measurement time.

As mentioned earlier, $\widehat{N}_{m,l}$ is defined by the FT of the time-domain noise divided by that of the source waveform. Thus, $\widehat{N}_{m,l}$ is used to compute the SNR in the simulation. A specific SNR at ω_m and an average SNR over ω_m are calculated using the random noise with the equations as follows (the SNRs are referred as SNR_m and SNR_a):

$$SNR_m = -10\log_{10}\left(\frac{1}{L}\sum_{l=1}^{L}|\widehat{N}_{m,l}|^2\right). \tag{30}$$

$$SNR_a = -10\log_{10}\left(\frac{1}{ML}\sum_{m=1}^{M}\sum_{l=1}^{L}|\widehat{N}_{m,l}|^2\right). \tag{31}$$

SNR_m and SNR_a represent the variation in the SNR along the angular frequencies and the representative SNR for a trial in the simulation, respectively.

First, the NN-SBL is applied to the CIR estimation when uniform noise power exists along the frequency components of the measurement, and the result from the NN-SBL is compared with that the result from the UN-SBL. Twenty multiple measurements ($L = 20$) were used for the estimation of the CIRs. The received signal with a random arrival time was contaminated with uniform random noise for each trial, which $\widehat{N}_P$ is a constant. An error is evaluated with the absolute difference of the true time delay from the estimated time delay that corresponds to the maximum amplitude from the SBL. The errors are calculated according to the various values of $\widehat{N}_P$ to examine the robustness of the SBLs (Fig. 1(a)). For a fixed $\widehat{N}_P$, the trial is repeated 50 times; the means of SNR_a and estimation error are values on the x and y axes of Fig. 1(a), respectively. While the noise that follows uniform distribution in the simulation deviates from the assumption of SBL (Gaussian distribution), the SBLs show superior performances as in [26], [27], and [28]. Some estimation results at SNRs less than −11 dB for both SBLs have the largest peaks at time delays that are different from the true values, which

increase the estimation error. As expected, the error becomes insignificant with an increase in the SNR (or a decrease in $\widehat{N}_P$). At the SNRs above −11 dB, the SBLs accurately estimate the time delays, and the estimation error becomes almost zero, which the order of error is 10^{-14} ms. Fig. 1(b) shows the CIR from the SBLs for a specific trial with an SNR_a of approximately −14 dB. While minor peaks appear and the maximum amplitude is considerably less than the true value of 1 in the CIR, the arrival can be clearly distinguished from the noise, and the time delay that corresponds to the maximum amplitude matched the true value (vertical dash-dotted line in Fig. 1(b)).

Fig. 1(c) includes the corresponding noise variances of the CIRs in Fig. 1(b). They are calculated using (27) and (28) for the NN-SBL and the UN-SBL, respectively. They are then compared with the measured noise variances based on (30). $\widehat{N}_P$ is independent of the frequency, so the measured noise variances fluctuate slightly around −14 dB, which is in good agreement with the results from the NN-SBL. The constant noise variances from the UN-SBL are located at the center of the fluctuation. While the NN-SBL requires more noise variances to be estimated using the EM algorithm with the same number of equality conditions, it delivers a performance that is similar to that the performance of the UN-SBL in the environment of uniform noise power due to the sufficient measurements, as shown in Fig. 1. The two SBLs show different trends in regards to estimating the CIRs under insufficient measurements. The NN-SBL underestimates the arrival amplitudes, which the opposite happens in the UN-SBL. Furthermore, the UN-SBL inclines to include the fake arrivals by noise due to the simplified uniform noise assumption. Each scheme has pros and cons when using insufficient measurements, which are shown in Fig. 6.

As described in (4), the noise with the TF is scaled by the FT of the source waveform, which incurs nonuniform noise variances over the measurement along the frequency.
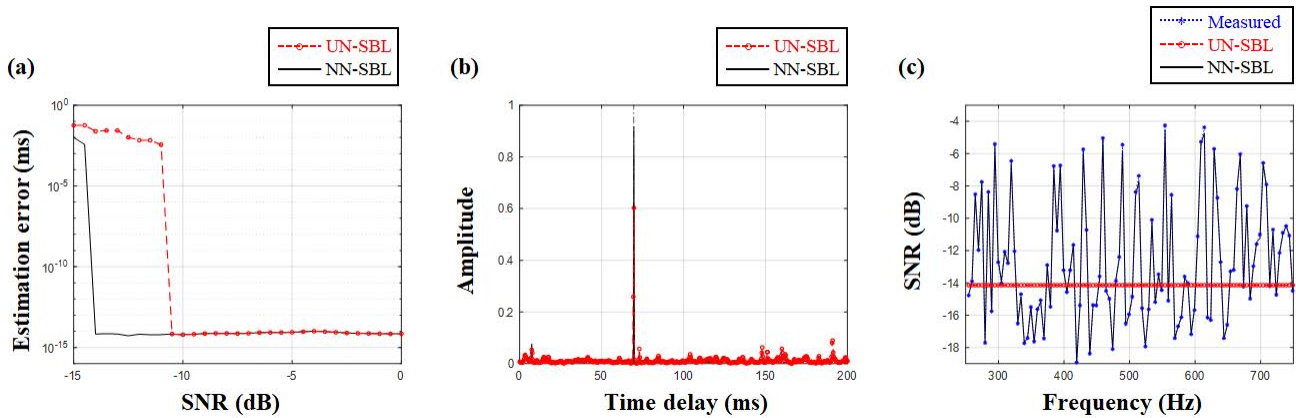
FIGURE 2. The UN-SBL and NN-SBL that use simulated data that includes noise with nonconstant variance over measurements along the frequency. An ideal TF is used for the simulation. (a) The mean estimation error evaluated with a difference between the true and the estimated time delays. At a low SNR, the NN-SBL results are better than the results with constant noise variance due to the selective use of relatively high SNR measurement components. (b) The CIRs from the SBLs at an SNR of approximately −14 dB. The vertical dash-dotted line indicates the true arrival. (c) The corresponding noise variances along the frequency, which are compared to the measured noise variances using (30).

A frequency-dependent $\widehat{N}_P(\omega_m)$ is used to generate the random noise, which is given by

$$\widehat{N}_P(\omega_m) = \widehat{N}_C(0.8U(0,1) + 0.2). \qquad (32)$$

$\widehat{N}_C$ determines the SNR of the trial. The constant, which is 0.2, ensures that SNR_m is not too large.

From Fig. 2(a), the NN-SBL, which considers different noise variances, outperforms the UN-SBL, which has the largest estimation errors at SNRs less than −11 dB, which occurred in the previous case. The NN-SBL also exhibits an improved result for inconsistent noise power, when compared with Fig. 1(a), where all the measurements over the frequency are corrupted by significant noise. However, in Fig. 2(a), the nonuniform noise variances induce relatively high SNRs in parts of the measurement, which is also illustrated in Fig. 2(c), and the NN-SBL can impose more priority on the high SNR measurements when evaluating the signal powers using the EM algorithm, which leads to a better result. In contrast, the UN-SBL cannot utilize the fine measurement components by treating the complex noise with the simple noise model, and its performance is similar to the performance that is illustrated in Fig. 1(a).

While the UN-SBL has a maximum peak, which corresponds to the true arrival time discriminated from minor peaks, it underestimates the arrival amplitude at a low SNR of approximately −14 dB (Fig. 2(b)). This problem is ameliorated by the NN-SBL exploiting the high SNR measurement components, which is shown in Fig. 2(c), where the noise powers oscillate significantly along the measurement. The noise variances from the NN-SBL are in good agreement with the measured noise variances, whereas they are simplified as a single value in the UN-SBL and deviate from the true values.

At this time, (2) is used for a more realistic simulation, where a chirp signal with a center frequency of 500 Hz (see Figs. 3(a) and 3(b)) randomly arrives at the receiver on the grids between 20 ms and 180 ms with additive white Gaussian

noise (AWGN) and outliers (intensive impulse signals). Three percentages of the simulated signal are the randomly emerging outliers, and their amplitudes follow uniform distribution between five and ten times the largest value of the transmitted signal. The ideal TF with a flat response along the frequency is substituted with a TF with an uneven response that reflects the frequency-dependent attenuation [30]. The amplitudes of the TF in the frequency band that are used for the estimation are random numbers that are uniformly selected between 0.9 and 1.1. The FT of the received signal divided by that of the chirp signal is the measurement, and 20 measurements are applied for the estimation via the SBLs. As shown in Fig. 3(c), considerable peaks in the MF result arising from the noise with the outliers are significantly diminished by the NN-SBL, whereas the sparse solution from the UN-SBL also provides a clearer CIR compared to the MF result, which the noticeable peaks remain, and they are detrimental to the accurate evaluation of the true arrival. The inset displays the difference between the NN-SBL and the UN-SBL results near the true arrival.

As expected, the source spectrum causes the AWGN to have different SNRs along the frequency (Fig. 3(d)). A source frequency component with a larger value tends to yield a higher SNR_m and vice versa, which results in SNR_m having a similar shape to that of the source spectrum.

B. BASIS-MISMATCH EFFECTS ON THE PERFORMANCE OF NONUNIFORM NOISE SBL

When a sound wave propagates in the ocean, it arrives at a receiver with a time delay in the continuous domain. Furthermore, the predefined on-grid bases (or columns) of the transformation matrix induce inevitable errors in the linear system. To mitigate the problem due to the basis match, a finer grid with a higher sampling frequency can be adopted, but it increases the computational burden as well as the similarity of the adjacent bases in the transformation matrix, which leads
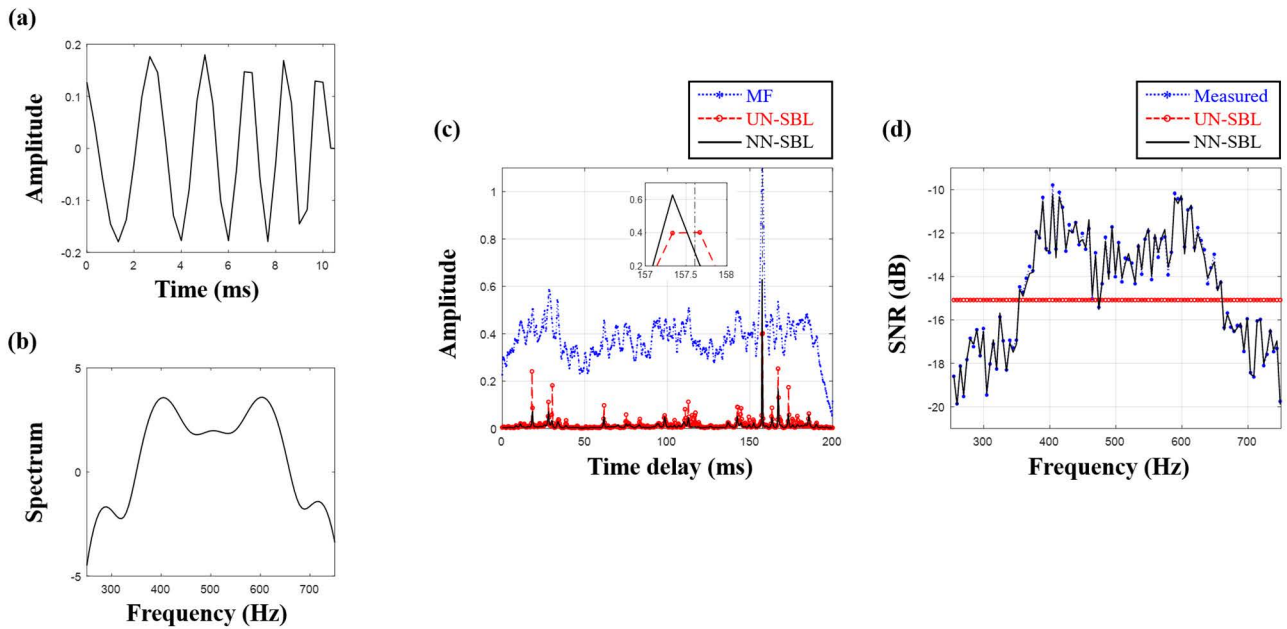
FIGURE 3. A chirp signal is used as a source waveform for the simulation, and additive white Gaussian noise (AWGN) with outliers is added to the simulated data for a realistic numerical experiment. An ideal TF is modified to reflect a frequency-dependence attenuation in the ocean. (a) A chirp signal that has a center frequency of 500 Hz, (b) a frequency response of the chirp signal, and (c) CIRs from the MF and SBLs at an SNR of approximately −15 dB. The vertical dash-dotted line denotes the true arrival. The considerable peaks in the MF result arise from the noise with the outliers, and they are significantly diminished by the SBLs (in particular, the NN-SBL). The inset displays the difference between the NN-SBL and the UN-SBL results near the true arrival. (d) The corresponding noise variances along the frequency, which are compared with the measured noise variances using (30). The measured noise variances resemble the frequency response of the chirp signal.

to a very inefficient way to solve the linear system. Alternatively, the first-order Taylor expansion for the linear system can be used [21], [22], where an additional unknown vector (N dimension) for the difference between a true off-grid time delay and an estimated on-grid time delay is evaluated.

While the basis mismatch hinders the exact estimation of the CIRs, an estimated arrival from the SBL appears near a true arrival due to the orthogonal-like bases of the linear system for the CIR estimation. Thus, an on-grid SBL is adopted in this study, which uses a sampling frequency that is associated with the desired time resolution at the cost of the estimation error.

The similarity of two bases calculated via their inner product after normalization is given by

$$S(\Delta n) = \left| \frac{1}{M} \sum_{m=0}^{M-1} e^{-j2\pi \frac{m}{N}\Delta n} \right| \approx \left| \mathrm{sinc}\left(\frac{M}{N}\Delta n \right) \right|,$$
(33)

where Δn is the index difference between the time delays that corresponds to the bases. sinc(x) is the normalized sinc function, which is defined as sinc$(x) = \sin \pi x / \pi x$. The exact expression for similarity is approximated with the assumption of $\Delta n \ll N$ for a convenient analysis. M/N is directly proportional to the ratio of the source frequency band to the largest frequency for the discretized signal, so the sinc function becomes sharp for a broadband source signal, which forms more orthogonal-like bases. The broadband source is

better for an SBL-based CIR estimation, which is similar to an MF.

The similarity decreases with an increase in Δn, which is shown in Fig. 4(a), and it includes similarities for all pairs of two columns in the transformation matrix, which is used for Figs. 1–3. Thus, the arrival with an off-grid time delay is represented by the bases near the arrival.

To demonstrate the orthogonal-like property of the bases in the CIRs, the estimation errors are computed using two different sampling frequencies of 3,000 Hz and 6,000 Hz, as shown in Fig. 4(b), where the chirp signal, as shown in Fig. 3, is used for the source waveform, and AWGN is added to the received signal that is computed from the convolution of the source waveform with the CIRs that have a time delay in the continuous domain as well as an uneven frequency response, as shown in Fig. 3. The overall estimation errors increase due to the basis mismatch as opposed to Fig. 2(a), where an ideal TF with an on-grid time delay is used for the simulation. However, the largest estimation error of 0.16 ms occurs at an SNR_a of −16 dB with a low sampling frequency. It is approximately half of the time difference between the two consecutive samples (sampling interval $\Delta t = 1/f_s$) discretized with a sampling frequency of 3,000 Hz. This indicates that the major arrivals that were estimated from the SBL are located near the true arrival even at the lowest SNR of the simulation. As the SNR increases, both estimation errors for the different sampling frequencies decrease and converge to 0.08 ms and 0.04 ms, which are equal to a

quarter of the sampling intervals that corresponds to the sampling frequencies of 3,000 Hz and 6,000 Hz. As previously mentioned, a time delay in the simulation is random in the continuous domain, and its absolute time difference from the closest discrete time delay is between 0 and $0.5\Delta t$. When the estimated arrivals from the SBL are on the nearest grids of true arrivals at a specific SNR_a, the average of their time delays becomes a quarter of the sampling interval due to the absolute time difference between the true and the estimated arrivals following a uniform distribution of $U(0, 0.5\Delta t)$. While the sampling frequency determines the time resolution with respect to the ability to separate the adjacent arrivals in the SBL, a low sampling frequency (coarse bases) does not result in the incorrect detection of a signal far from the true arrival. The SBL can determine the best solution of the linear system at a sufficient SNR, and it is irrespective of the sampling frequency, as shown in Fig. 4(b). It also suffers less from the basis mismatch, which is unlike the sparse signal reconstruction-based beamforming [9], [13], [14], [15], [21], [22], [23], [24], [25], [26], [27].

C. EXAMINING TIME RESOLUTION OF NONUNIFORM NOISE SBL AT LOW FREQUENCY

When transmitting and receiving sound waves in a water tank, a low-frequency source waveform with a limited frequency band is not preferred due to the insufficient pulse compression that prevents the separation of the arrivals that are in close proximity. However, to investigate the low-frequency acoustic impedance of a submerged object in a water tank, a low-frequency source is indispensable, and a scheme to overcome the problem of the MF is required, which is the motivation for the present study.

To examine the time resolution of the NN-SBL at low frequencies, a numerical experiment to distinguish two adjacent arrivals is conducted. In the numerical experiment, a transducer and a hydrophone are 2 m and 1 m away from the center of the rigid target (thin steel plate with 1.5 m × 1.5 m), respectively. Also, the sound speed of the surrounding target is constant at 1500 m/s, and the high- and the low-frequency Hanning-weighted four period sine signals that have the same frequency bands as their center frequencies are used as the source waveforms, in which is similar to the study that was conducted by Choo and Song [31] that enabled a convenient comparison of the time resolutions at two different source frequencies (1 kHz and 10 kHz). To simulate a scattered signal from the target, the Helmholtz integral was used with the Kirchhoff approximation for both frequencies, which was valid in the high-frequency region. Equation (4) in Ref. [31] was modified to account for the rigid boundary condition of the target.

AWGN is added to the noise-free time-domain simulated signals. Fifty trials were repeated with randomly generated noise for each source signal, which twenty multiple measurements were used for each trial for the estimations, and the estimation means from the MF and SBLs are presented in Fig. 5. They are normalized with their maximum values
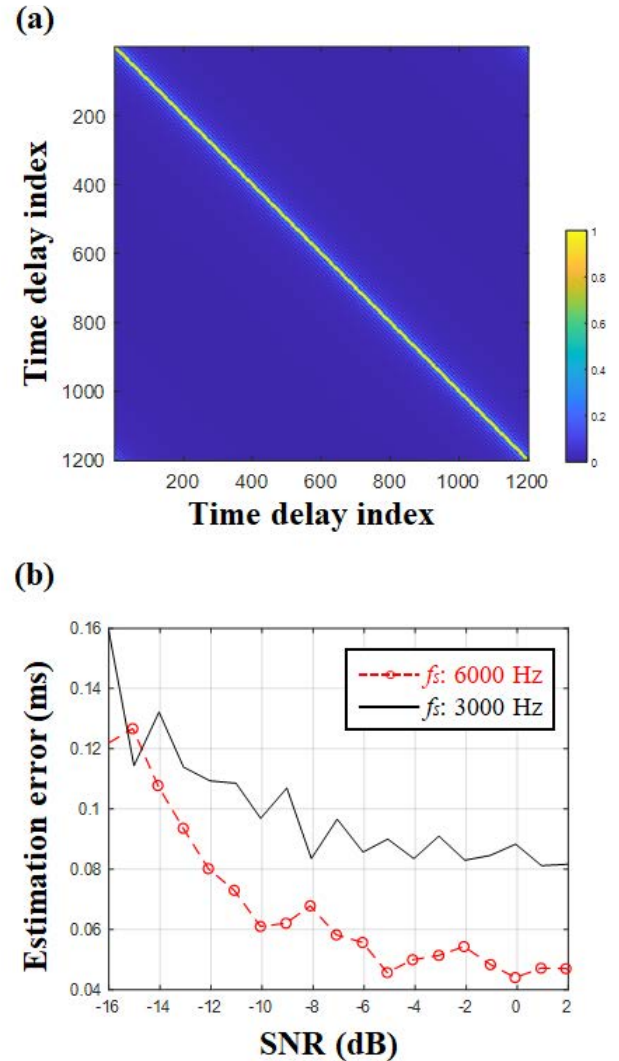

FIGURE 4. (a) Gram matrix displaying similarities of columns in the transformation matrix for Figs. 1–3. The similarity decreases with increase in distance between the columns, which makes the Gram matrix resemble the identity matrix. (b) The mean estimation error according to the SNR for simulations using different sampling frequencies of 3,000 Hz and 6,000 Hz. Off-grid arrival times in the simulation lead to a basis mismatch resulting in performance degradation of the NN-SBL. However, the orthogonal-like columns enable the NN-SBL to have the estimated arrivals near the true ones even at the lower sampling frequency with less time resolution.

for a convenient comparison, where both SNR_a high and low frequencies are approximately −4.5 dB. In particular, the existing SBLs [26], [27], which can treat heteroscedastic noise, are applied to the same data for a comparison, which are hereinafter referred to as heteroscedastic-noise SBL (HN-SBL). The vertical dash-dotted lines indicate the true arrival time delays that correspond to the direct (the first) and the scattered (the second) signals.

At high frequencies (sampling frequency of 80 kHz), the MF can separate two arrivals due to the broadband signal whereas the overall offsets are induced by the noise. The noise also weakened the second arrival from the UN-SBL,
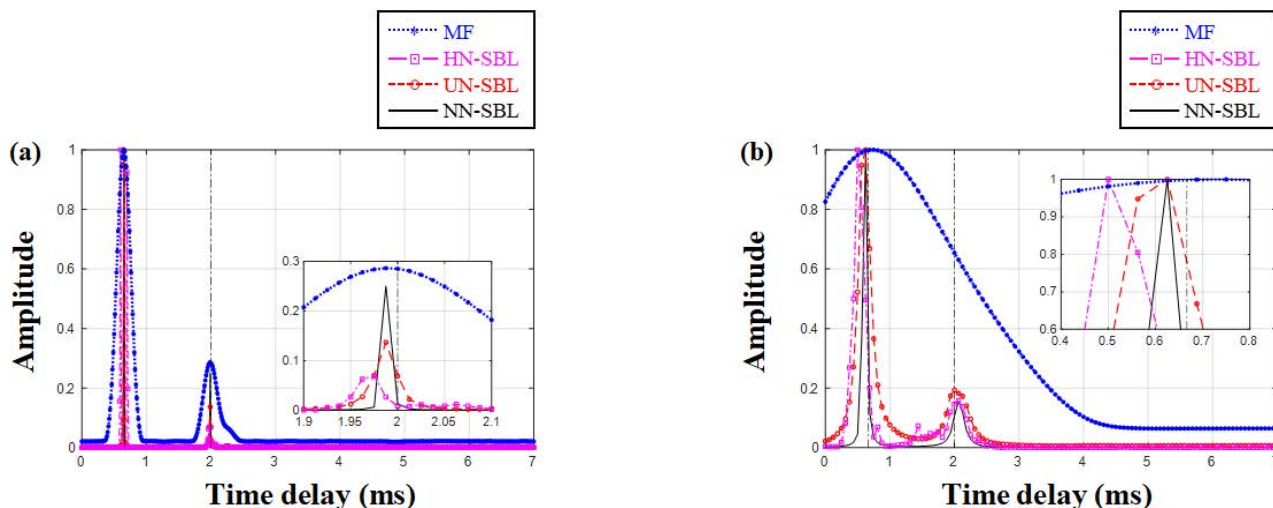
FIGURE 5. The high frequency (10 kHz) and low frequency (1 kHz) synthetic acoustic data are contaminated by additive white Gaussian noise (AWGN), and the SNR is approximately −4.5 dB. (a) The mean estimation results from the MF, UN-SBL, NN-SBL, and HN-SBL at 10 kHz. The AWGN deteriorates the performances of the SBLs. The direct arrival is divided into two arrivals in HN-SBL. Furthermore, as shown in the inset, the noise weakens the scattered signals in the SBL results. In particular, the scattered signals from the HN-SBL are distributed over the time delay, and it results in the weakest scattered signal. On the other hand, the NN-SBL recovers the arrivals clearly from the contaminated synthetic data, whereas the amplitude of the scattered signal is slightly reduced. (b) The mean estimation results from the MF, UN-SBL, NN-SBL, and HN-SBL at 1 kHz. At a low frequency, the estimation results are different according to the trials, and their mean is spread over the time delay, so the UN-SBL results are more distributed, which makes the mean blunt. Furthermore, the first arrival from the HN-SBL is considerably deviated from the true one, which is displayed in the inset, and the fictitious peak emerges ahead of scattered signal. As in the high frequency case, the NN-SBL demonstrates the best performance among the SBLs.

whereas that the second arrival from the NN-SBL remained almost the same due to the exploitation of the fair measurement components. While the major arrivals from the HN-SBL are near the true ones, the direct arrival in the synthetic data is divided into two arrivals, and the amplitude of the scattered signal is evaluated to be significantly lower than the true value, as displayed in the inset of Fig. 5(a). The NN-SBL exhibits the best performance in regards to handling the nonuniform noise at a high frequency. Meanwhile, at the high frequency, the MF can distinguish the two arrivals by the sufficient source bandwidth and the sophisticated approaches like the SBLs are unnecessary. Thus, most examinations for the CIR estimation in the present study were conducted at low frequency regions that included the following experiments, where the MF suffers from separating adjacent arrivals and the advanced schemes are required.

At a low frequency (sampling frequency of 16 kHz), the narrower frequency band deteriorates the estimation of the time delay. The MF cannot distinguish the direct and the scattered arrivals (overlapped two arrivals) due to a narrower frequency band (one tenth of that the frequency band for the high frequency) inducing the insufficient time resolution. The SBLs enable the arrivals to be separated due to their sparse solutions. However, the UN-SBL results are inconsistent according to the trials, which makes the mean estimation widespread over a time delay. Furthermore, the HN-SBL estimates the first arrival that is the farthest from the true one, as displayed in the inset of Fig. 5(b), and the fictitious peak emerges ahead of the scattered signal. The deterioration is mitigated by the NN-SBL, which estimates the arrivals

more consistently along the trials and displays the higher time resolution with the sharpened arrival evaluations. The estimations are within one sample from the closest samples to the true arrivals and provide the most useful information among the schemes.

It is worth noting that the conventional SBL is corrected to treat the heteroscedastic noise heuristically in Refs. [26] and [27], and the performance degradation might be attributed to the heuristic derivation. In this study, the rigorous expansion of the conventional SBL is derived to consider the nonuniform noise exactly, which leads to the clearest CIR estimation among the SBLs.

V. APPLYING NONUNIFORM NOISE SBL TO THE IN-SITU DATA

A. REAL MEASUREMENT DATA IN THE OCEAN: SAVEX15

The shallow-water acoustic variability experiment 2015 (SAVEX15) was conducted in the northeastern East China Sea [32], and the sound waves that were traveling within a shallow acoustic waveguide were measured at high and low frequencies. In this study, the low-frequency signals, which were recorded with a sampling frequency of 100 kHz, were used to examine the NN-SBL by comparing its results with the results from the MF and the existing SBLs, such as the UN-SBL and the HN-SBL.

When measuring the low-frequency signal, a transducer at a depth of 50 m transmitted a 100 ms-length linear frequency modulated (LFM) pulse waveform with a frequency band in the range of 0.5–2 kHz, and a vertical line array (VLA) that was comprised of evenly spaced 16 hydrophones (3.75 m)
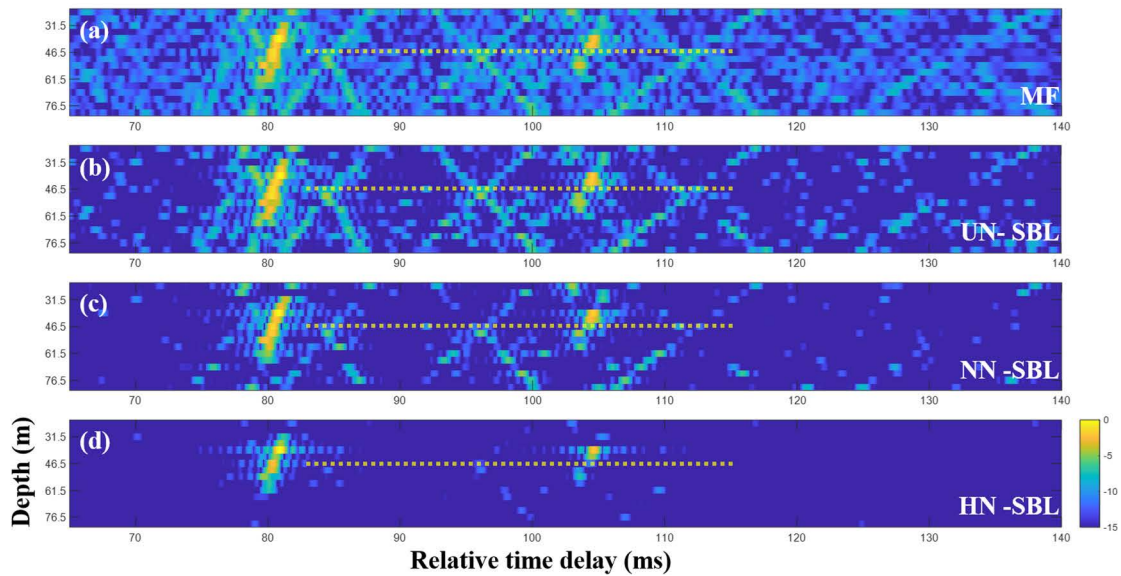
FIGURE 6. The CIRs along depths of the sensors in vertical line array (VLA): (a) MF, (b) UN-SBL, (c) NN-SBL, and (d) HN-SBL. A single acoustic measurement is used for the estimation. The schemes are more sophisticated, so the acoustic structures (e.g., 'x' shapes that are formed by the upward and downward incoming arrivals to the VLA) are observed more clearly. The noise in the MF result is noticeably removed in the SBL results. In particular, the most possible arrivals remain in the NN-SBL result at the cost of their weakening due to the insufficient measurement. Meanwhile, the HN-SBL estimates the CIRs too sparsely and filters out almost all the true arrivals except for intensive arrivals in the middle of the water column. Afterwards, the CIRs around the dotted lines are used for a performance comparison in terms of resolution and reestablishment of the CIR from the measurement.

was separated from the transducer at a distance of approximately 1.8 km for the recording. Different waveforms for underwater communications were subsequently transmitted from the transducer, so a single measurement for the LFM signal is available to estimate the CIRs of the SAVEX15.

B. ESTIMATED CHANNEL IMPULSE RESPONSE OF SAVEX15

To demonstrate the usability and feasibility of the NN-SBL in the CIR estimation, it was applied to the real measurement data, and the results were compared with the results from the other schemes. The MF was applied to the VLA data, whereas the UN-SBL, NN-SBL, and HN-SBL were applied to the VLA data after the downsampling to avoid the computational burden with a small N in (5). A sampling interval of 10 in the original VLA data was used for the SBLs, and the sampling frequency is reduced to 10 kHz, which is sufficient to prevent aliasing at a low frequency. The CIRs along the hydrophone depths produced acoustic structures by the waveguide, which included the 'x' shapes that were formed by the incoming arrivals to the VLA from the upward and downward directions. They appeared more clearly with the improvement of the scheme (Fig. 6). The source waveform is cross-correlated with the VLA data in the MF, and the corresponding envelopes, which were based on the Hilbert transform, were used for the CIRs. This process leads to pulse compression for the LFM signal and allows for better observation of the acoustic structures with higher time resolutions as well as noise reduction. In contrast, the

SBLs inherently derive a high-resolution CIR with less noise by solving the linear system of (5). For the visualization in this study, the SBL results were purposely convolved with an autocorrelation of the LFM signal, and the corresponding envelopes were used, which is illustrated in Fig. 6. The direct results for the SBLs were subsequently compared with the results from the MF in Fig. 7.

While the arrivals around 80 ms and 105 ms have high intensities due to the refractive sound speed profile in the SAVEX15, the arrivals that form the 'x' shapes are more focused on the performance comparison. The major arrivals were found to use the MF, but they entailed noise overall. The noise around the 'x' shapes caused the arrivals to appear stretched over the relative time delay. The noise near the lower left part of the second 'x' shape masked the arrivals. These are detrimental to the clear detection of the arrival directions to the VLA when time-domain beamforming is performed. The SBLs tend to select bases of the transformation matrix that correspond to the actual arrivals, so the noise in the measurement is suppressed during the iterative estimation of the signal powers in the SBLs. Thus, in the UN-SBL result, the noise is remarkably removed, and the masked arrivals around the second 'x' shape are more clearly observed. The performance in terms of the noise reduction is improved by the extended SBL, which is due to the more complex approach to noise in the measurement. Most of the noise in the MF result is diminished with the more advanced scheme, as shown in Figs. 6(a) and 6(c). This is achieved at the cost of the weakened arrivals. The NN-SBL estimates multiple
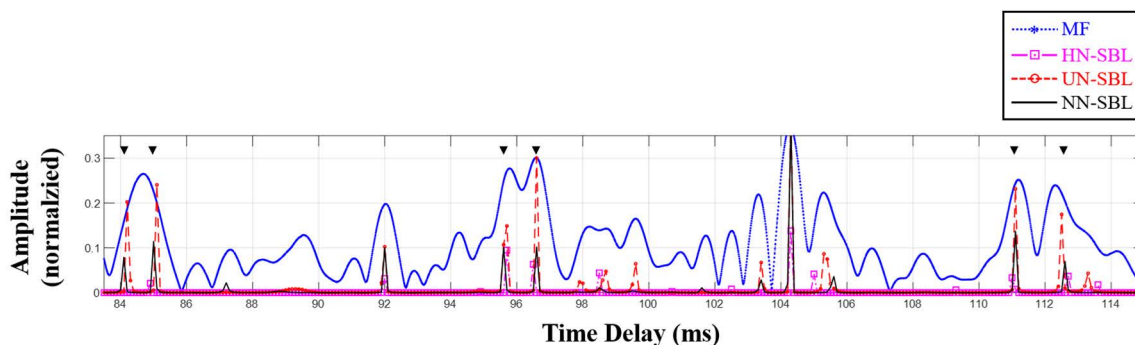
FIGURE 7. The CIRs around the dotted lines in Fig. 6. The triangles indicate the arrivals from the upward and downward directions. The closest arrivals that are not resolved by an MF can be separated by both the UN-SBL and NN-SBL. As expected, most of the noise in the MF result is cleared by the NN-SBL, which is traded with the weakened arrivals. On the other hand, the arrivals are too diminished in the HN-SBL result. In particular, the arrival near 84 ms that comprise of the acoustic structure of 'x' shape is absent.

noise powers according to the frequencies here using a single measurement. This should not be sufficient for an accurate estimation, and it induces the weak arrivals. The HN-SBL estimates the CIRs too sparsely and filters out almost all the true arrivals except for the intensive arrivals in the middle of the water column. The upward and downward arrivals that form the 'x' shapes are either absent or weakly present.

As mentioned before, the 'x' shapes are formed by the upward and downward incoming arrivals getting closer at first and farther apart afterwards, which are merged at the VLA center. The measured signal at the sensor just above the center is used to examine the performance of the schemes in terms of the time resolution. Figure 7 shows parts of the CIRs from the MF and the SBLs that correspond to the dotted lines in Fig. 6. The MF result and the direct estimates from the SBLs are used here for the comparison after the normalization.

The triangles indicate the arrivals that are relevant to the 'x' shapes. The MF cannot distinguish the closest two arrivals near 85 ms, which is due to the lower time resolution by an insufficient frequency band at a low frequency, whereas the sparse estimations of the SBLs enable the arrivals to be separated, which included the other arrivals. The noise in the MF result, which has an intensity that is comparable to that the intensity of the arrivals, is noticeably reduced by the SBL-based CIR estimators (more by the NN-SBL). On the other hand, the arrivals are too diminished in the HN-SBL result. The arrival near 84 ms that comprised of the acoustic structure of the 'x' shape is absent, and it hinders the recovery of the true CIR from the measurement.

VI. SUMMARY
The MF that generally uses the cross-correlation of the source waveform with the measured signal is used to estimate a CIR that display the arrivals via the pulse compression and the suppression of uncorrelated noise. However, its application is limited by the insufficient frequency band of the source waveform, which leads to the broadening of the arrivals, which makes it difficult to distinguish the adjacent arrivals. The SBL, which was originally developed for classification

and regression, was extended to estimate a high-resolution CIR with a limited frequency band.

In this study, the SBL was used to solve a linear system of CIRs, which were established by the physics of underwater sound propagation. The omnipresent noise was scaled using the source spectrum, which resulted in nonuniform noise powers in the measurement violating a basic assumption in the conventional SBL. To treat the inconsistent noise, the SBL was expanded mathematically to accommodate the noise, which was examined using simulated data that included a single arrival. The expanded SBL (referred to as the NN-SBL) delivered a superior performance with a more apparent arrival estimation than the existing SBLs (referred to as the UN-SBL and the HN-SBL) at a low SNR.

An inherent problem of the SBL is the basis mismatch that was caused by the discretized columns corresponding to the on-grid arrival times that did not precisely match the true off-grid arrival times. The orthogonal-like bases of the transformation matrix in the linear system fortunately ensure that the estimated arrival is close to the true value. The synthetic data, which was sampled with two different sampling frequencies, was used to support the properties of the bases. The NN-SBL has an arrival around the true one even at a low sampling rate with less time resolution.

A numerical experiment was conducted to demonstrate the high-resolution CIR via the SBLs, where a scattered signal from a finite submerged target was simulated with the direct arrival. When a low-frequency source was used with a frequency band of 1 kHz, the MF could not distinguish between the two arrivals with a travel distance difference of 2 m, which was due to its low time resolution being proportional to the source frequency band. On the contrary, the SBLs separated the scattered signal from the direct signal via the sparse estimation of the CIR linear system. The NN-SBL exhibited a better noise-reduction performance when the multiple measurements that were obtained over time were available.

The extended SBL was applied to the SAVEX15 data that was measured using a VLA at low frequencies (0.5–2 kHz) with the other schemes (MF, UN-SBL, and

HN-SBL). The noise smearing actual arrivals in the MF result was remarkably diminished by improving the schemes. While the arrivals are weakened by the insufficient measurements in the CIRs from the NN-SBL, it retained the highest possible arrivals and provided the most apparent estimation. Furthermore, the time resolution via the SBL was examined with the received signal that was measured by the sensor just above the VLA center, which had close arrivals from the upward and downward directions before the merging. As expected, all the close arrivals were separated with less noise using the sparse estimation.

REFERENCES

[1] A. H. Quazi, "An overview on the time delay estimate in active and passive systems for target localization," *IEEE Trans. Acoust., Speech, Signal Process.*, vol. ASSP-29, no. 3, pp. 527–533, Jun. 1981.
[2] D. A. Abraham, *Underwater Acoustic Signal Processing: Modeling, Detection, and Estimation*. Cham, Switzerland: Springer, 2019.
[3] K. Gedalyahu and Y. C. Eldar, "Time-delay estimation from low-rate samples: A union of subspaces approach," *IEEE Trans. Signal Process.*, vol. 58, no. 6, pp. 3017–3031, Jun. 2010.
[4] E. J. Candès and M. B. Wakin, "An introduction to compressive sampling," *IEEE Signal Process. Mag.*, vol. 25, no. 2, pp. 21–30, Mar. 2008.
[5] D. L. Donoho, "Compressed Sensing," *IEEE Trans. Inf. Theory*, vol. 52, no. 4, pp. 1289–1306, Jan. 2006.
[6] C. R. Berger, Z. Wang, J. Huang, and S. Zhou, "Application of compressive sensing to sparse channel estimation," *IEEE Commun. Mag.*, vol. 48, no. 11, pp. 164–174, Nov. 2010.
[7] C. Ekanadham, D. Tranchina, and E. P. Simoncelli, "Recovery of sparse translation-invariant signals with continuous basis pursuit," *IEEE Trans. Signal Process.*, vol. 59, no. 10, pp. 4735–4744, Oct. 2011.
[8] K. Fyhn, M. F. Duarte, and S. H. Jensen, "Compressive parameter estimation for sparse translation-invariant signals using polar interpolation," *IEEE Trans. Signal Process.*, vol. 63, no. 4, pp. 870–881, Feb. 2015.
[9] G. F. Edelmann and C. F. Gaumond, "Beamforming using compressive sensing," *J. Acoust. Soc. Amer.*, vol. 130, no. 4, pp. EL232–EL237, Oct. 2011.
[10] P. Gerstoft, C. F. Mecklenbräuker, W. Seong, and M. Bianco, "Introduction to compressive sensing in acoustics," *J. Acoust. Soc. Amer.*, vol. 143, no. 6, pp. 3731–3736, Jun. 2018.
[11] P. Gerstoft, A. Xenaki, and C. F. Mecklenbrauker, "Multiple and single snapshot compressive beamforming," *J. Acoust. Soc. Amer.*, vol. 138, no. 4, pp. 2003–2014, Oct. 2015.
[12] Y. Park, W. Seong, and Y. Choo, "Compressive time delay estimation off the grid," *J. Acoust. Soc. Amer.*, vol. 141, no. 6, pp. EL585–EL591, Jun. 2017.
[13] Y. Park, Y. Choo, and W. Seong, "Multiple snapshot grid free compressive beamforming," *J. Acoust. Soc. Amer.*, vol. 143, no. 6, pp. 3849–3859, Jun. 2018.
[14] A. Xenaki and P. Gerstoft, "Grid-free compressive beamforming," *J. Acoust. Soc. Amer.*, vol. 137, no. 4, pp. 1923–1935, 2015.
[15] A. Xenaki, P. Gerstoft, and K. Mosegaard, "Compressive beamforming," *J. Acoust. Soc. Amer.*, vol. 136, no. 1, pp. 260–271, Jul. 2014.
[16] C. R. Berger, S. Zhou, J. C. Preisig, and P. Willett, "Sparse channel estimation for multicarrier underwater acoustic communication: From subspace methods to compressed sensing," *IEEE Trans. Signal Process.*, vol. 58, no. 3, pp. 1708–1721, Mar. 2010.
[17] S.-H. Byun, W. Seong, and S.-M. Kim, "Sparse underwater acoustic channel parameter estimation using a wideband receiver array," *IEEE J. Ocean. Eng.*, vol. 38, no. 4, pp. 718–729, Oct. 2013.
[18] W. Li and J. C. Preisig, "Estimation of rapidly time-varying sparse channels," *IEEE J. Ocean. Eng.*, vol. 32, no. 4, pp. 927–939, Oct. 2007.
[19] Y. Choo, Y. Park, and W. Seong, "Detection of direction-of-arrival in time domain using compressive time delay estimation with single and multiple measurements," *Sensors*, vol. 20, no. 18, p. 5431, Sep. 2020.
[20] M. E. Tipping, "Sparse Bayesian learning and the relevance vector machine," *J. Mach. Learn. Res.*, vol. 1, no. 9, pp. 211–244, Aug. 2001.
[21] A. Das, "Theoretical and experimental comparison of off-grid sparse Bayesian direction-of-arrival estimation algorithms," *IEEE Access*, vol. 5, pp. 18075–18087, 2017.
[22] A. Das and T. J. Sejnowski, "Narrowband and wideband off-grid direction-of-arrival estimation via sparse Bayesian learning," *IEEE J. Ocean. Eng.*, vol. 43, no. 1, pp. 108–118, Jan. 2018.
[23] P. Gerstoft, C. F. Mecklenbrauker, A. Xenaki, and S. Nannuru, "Multi-snapshot sparse Bayesian learning for DOA," *IEEE Signal Process. Lett.*, vol. 23, no. 10, pp. 1469–1473, Oct. 2016.
[24] X. Wu, W.-P. Zhu, and J. Yan, "Direction of arrival estimation for off-grid signals based on sparse Bayesian learning," *IEEE Sensors J.*, vol. 16, no. 7, pp. 2004–2016, Apr. 2016.
[25] Z. Yang, L. Xie, and C. Zhang, "Off-grid direction of arrival estimation using sparse Bayesian inference," *IEEE Trans. Signal Process.*, vol. 61, no. 1, pp. 38–43, Jan. 2013.
[26] P. Gerstoft, S. Nannuru, C. F. Mecklenbräuker, and G. Leus, "DOA estimation in heteroscedastic noise," *Signal Process.*, vol. 161, pp. 63–73, Aug. 2019.
[27] S. Nannuru, K. L. Gemba, P. Gerstoft, W. S. Hodgkiss, and C. F. Mecklenbräuker, "Sparse Bayesian learning with multiple dictionaries," *Signal Process.*, vol. 159, pp. 159–170, Jun. 2019.
[28] K. Huang and Z. Yang, "Robust sparse Bayesian learning for sparse signal recovery under unknown noise distributions," *Circuits, Syst., Signal Process.*, vol. 40, pp. 1365–1382, Mar. 2021.
[29] M. G. Wenz, "Acoustic ambient noise in the ocean: Spectra and sources," *J. Acoust. Soc. Amer.*, vol. 34, no. 12, pp. 1936–1956, Dec. 1962.
[30] F. B. Jensen, W. A. Kuperman, M. B. Porter, and H. Schmidt, *Computational Ocean Acoustics*. New York, NY, USA: Springer, 2011.
[31] Y. Choo and H. C. Song, "Comment on 'reconstructing surface wave profiles from reflected acoustic pulses' [J. Acoust. Soc. Am. 133(5), 2597–2611 (2013)]," *J. Acoust. Soc. Amer.*, vol. 139, no. 5, pp. 2399–2402, May 2016.
[32] H. Song, C. Cho, W. Hodgkiss, S. Nam, S.-M. Kim, and B.-N. Kim, "Underwater sound channel in the northeastern east China sea," *Ocean Eng.*, vol. 147, pp. 370–374, Jan. 2018.

YOUNGMIN CHOO (Member, IEEE) was born in Jinju, South Korea, in 1981. He received the B.A. degree in engineering and the Ph.D. degree in underwater acoustics from Seoul National University, South Korea, in 2005 and 2012, respectively. He completed the Postdoctoral Fellowships at Seoul National University and Scripps Institution of Oceanography, from 2012 to 2016, respectively. He has been an Assistant Professor at the Department of Defense Systems Engineering, Sejong University, since 2016, where he is currently an Associate Professor. He has particular research interests in the areas of signal processing and underwater acoustics. His main research interests include scattering and reverberation from rough boundaries, sonar signal processing of beamforming, and ocean parameter inversion from data.

HAESANG YANG (Member, IEEE) received the B.S. and Ph.D. degrees in naval architecture and ocean engineering from Seoul National University, Seoul, South Korea, in 2010 and 2016, respectively. He is currently a Research Assistant Professor with the Department of Naval Architecture and Ocean Engineering, Seoul National University. His research interests include acoustic signal processing, acoustic propagation modeling, and machine-learning applications in acoustic, vibration, and noise problems.

● ● ●